

# Topologically-protected metallic states induced by a one-dimensional extended defect in a 2D topological insulator

E. N. Lima

*Departamento de Física, ICEx, Universidade Federal de Minas Gerais,  
Avenida Antônio Carlos 6627, Pampulha, 30123-970, Belo Horizonte, MG, Brazil\**

T. M. Schmidt

*Instituto de Física, Universidade Federal de Uberlândia,  
Caixa Postale 593, 38400-902, Uberlândia, MG, Brazil*

R. W. Nunes

*Departamento de Física, ICEx, Universidade Federal de Minas Gerais,  
Avenida Antônio Carlos 6627, Pampulha, 30123-970, Belo Horizonte, Minas Gerais, Brazil†*

We report *ab initio* calculations showing that a single one-dimensional extended defect can originate topologically-protected metallic states in the bulk of two-dimensional topological insulators. We find that a narrow extended defect composed of periodic units consisting of one octagonal and two pentagonal rings embedded in the hexagonal bulk of a bismuth bilayer introduces two pairs of one-dimensional Dirac-fermion states with opposite spin-momentum locking. Although both Dirac pairs are localized along the extended-defect core, their interactions are screened due to the trivial topological nature of the extended defect.

Topological insulators (TIs) are a new class of materials theoretically predicted to exist in 2005 [1, 2], with the first experimental confirmation in HgTe/CdTe quantum wells reported in 2007 [3–5]. TIs have since been subject of intensive theoretical [4, 5] and experimental [6] studies due to the coexistence of an insulating bulk band structure with a non-trivial topology that, when interfaced with a topologically trivial insulator such as the vacuum, gives rise to time-reversal-protected metallic surface states, with Dirac-fermion dispersions spanning the bulk band gap in the one-dimensional (1D) edges in two-dimensional (2D) TIs. Existence of the edge states is a requirement imposed by the different topologies of the band structures across the interface. In these edge states, the spin quantization axis and the momentum direction are locked-in, implying that the metallic edge states are protected from backscattering, rendering their electronic conductance robust against the presence of disorder. Robust conduction and spin polarization may allow the manipulation of edge modes of TIs in many applications such as spintronics [7] and quantum computation [4, 5].

While topological-insulating band structures are also found in three-dimensional (3D) systems, manipulation of the metallic surface modes in 3D TIs is commonly hampered by the difficulty in tuning the Fermi level to achieve sufficiently low (ideally null) levels of bulk carriers, and the metallic surface carriers are significantly outnumbered by bulk carriers in most 3D TI samples [8, 9]. Hence, 2D TIs can be advantageous in transport applications, because the 2D bulk is fully exposed to chemical manipulation and, besides, the bulk Fermi level can also be tuned by proper gating. When an insulating bulk is achieved, electrons can conduct only along the edge in these structures. From this, many efforts have been

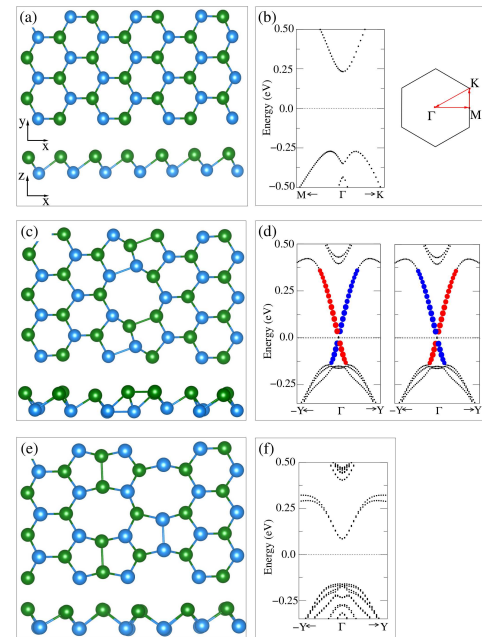


FIG. 1: (a) Top and side view of a pristine Bi bilayer. (b) Electronic band structure of a pristine Bi bilayer. (c) Top and side view of a Bi bilayer with an embedded 558 defect (BiBL+558 in the text). (d) Band structure of BiBL+558, showing Dirac-fermion metallic modes; spin-momentum locking is displayed: blue (red) branch of Dirac modes corresponds to spin 'up' ('down'). (e) Top and side view of a Bi bilayer with an embedded quadrupole-pentagon double-octagon defect (BiBL+Q5D8 in the text); (f) Band structure of Bi+Q5D8. In all geometries, atoms in the upper (lower) Bi triangular sub-lattice are shown as green (blue) circles.

made to find candidate 2D TI systems.

In this work, we show, by means of *ab initio* density functional theory (DFT) calculations, the formation of “edge-like” 1D metallic electronic states localized on the core of an extended 1D defect embedded in the bulk of a single (111)-oriented bismuth bilayer (BiBL). We show that in this system the extended defect implies the formation of two pairs of topologically-protected Dirac-fermion modes, each pair localized on each one of the two zigzag edges meeting at the core of the 1D extended defect. The Dirac pairs are shown to interact via a strongly screened interaction, and to have opposite chiralities, which in principle allows for backscattering of carriers propagating in these defect-induced modes.

Furthermore, we also introduce an alternative crystalline form of a Bi bilayer, consisting entirely of pentagonal and octagonal rings, which we refer to as the pentaoctite form of a BiBL. Below, we show that the pentaoctite BiBL, with a formation energy that is only 0.045 eV/atom larger than the bulk-derived hexagonal pristine layer, is also a 2D topological insulator.

Our calculations show that the occurrence of spin-polarized Dirac-fermion electronic states localized on the core of the extended line defect, which is fully immersed in the bulk of the 2D TI BiBL, is closely related to the emergence of metallic states along the edges of sufficiently large zigzag-terminated bismuth nanoribbons (ZBiNR). The 1D extended defect in our study is a buckled version of the so-called 558-defect, composed of periodic units consisting of one octagonal and two pentagonal rings, as shown in Fig.1(c). A flat version of the 558-defect has been shown experimentally to occur in graphene monolayers [10, 11], and theoretically to display magnetic quasi-1D electronic states in n-doped layers [12, 13].

While the possible occurrence of metallic fermionic modes along the core of 1D extended defects (dislocations) in 3D TIs has already been predicted theoretically for a model tight-binding hamiltonian for a 3D TI, [14] to the best of our knowledge, this work provides the first demonstration, by *ab initio* calculations, of the emergence of topologically-dictated helical Dirac-fermion states along the core of a 1D extended defect immersed in the bulk of a 2D TI.

Structural and electronic properties of extended 1D defects in a BiBL, in the present work, are computed using the DFT scheme implemented in the VASP code [15]. The projector-augmented-wave method [16] is used to describe the ionic core-valence electron interactions. The generalized gradient approximation (GGA) is employed to describe the exchange and correlation potential. [17] Spin-orbit coupling is included in the calculation of the electronic structure. Wave functions are expanded in plane waves with energy cutoff of 300 eV. Convergence with respect to the energy cutoff was carefully checked from calculations with cutoffs in the 200-400 eV range. Geometries are optimized until the forces on each atom are less than 0.03 eV/Å. Convergence with respect to

Brillouin zone (BZ) sampling was also verified.

It is well established that a single (111) Bi bilayer in its pristine form, shown in Fig.1(a), is a 2D TI (a quantum spin Hall system) [18–22]. Metallic edge states are found at the borders of a BiBL finite sheet, with a pair of helical Dirac fermion states with opposite spin textures (or spin-momentum locking) on each border [23]. The lower panel in Fig.1(a) shows that the BiBL is formed from two Bi 2D triangular sublattices displaced by 1.74 Å along the (111) direction (the *z*-axis in our supercells). Figure 1(b) shows the insulating band structure of an infinite pristine BiBL (thus devoid of edges) along the  $\Gamma$ -K and  $\Gamma$ -M lines in the Brillouin zone, with a band gap of  $\sim 0.5$  eV, within the GGA approximation. The top of the valence band at the  $\Gamma$  point is  $\sim 0.1$  eV below the absolute maximum of the valence band, so the direct gap at  $\Gamma$  is  $\sim 0.6$  eV.

The structure of the 558-defect embedded in a (111) BiBL is illustrated in Fig. 1(c). The 558-defect is a zigzag-oriented (along the *y*-axis of the cell) translational grain boundary between two crystalline domains shifted with respect to each other by one-third of the lattice period along the armchair direction (the *x*-axis of the cell). The relative shift leaves a seam between the two domains that is filled with a roll of Bi dimers, thus forming the two-pentagon-one-octagon periodic unit of the defect. The period of the 558-defect is twice the lattice constant of the pristine BiBL ( $a = 4.33$  Å). In the following, we shall refer to the BiBL with the embedded 558-defect as BiBL+558. After relaxation, the BiBL+558 system retains the buckled structure of the pristine BiBL. The Bi-Bi bond length in a pristine BiBL is 3.04 Å. In the pentagonal and octagonal rings of the BiBL+558 bond-length values range from 3.03 Å to 3.11 Å.

Figure 1(d) shows the band structure of the supercell for the BiBL+558 system. Inclusion of the 558-defect leads to the emergence of two degenerated pairs of edge modes, one on each side of the dimers, with linear dispersions and the characteristic spin textures of 2D TI edge modes. Note that the edge-state bands span the band gap of the insulating bulk BiBL. Figure 1(d) shows that the Dirac dispersions on both sides of the defect have opposite spin textures, with spin ‘up’ (‘down’) states moving ‘up’ (‘down’) on the left side of the dimers and ‘down’ (‘up’) on the right side of the dimers. Hence, the two zigzag lines of Bi atoms at the core of the 558 defect behave as right and left ribbon edges, preserving the “handedness” of each edge, which explains the inversion of the spin texture between the two sides of the Bi dimers.

This is an important point concerning the spin transport of the Dirac modes along the core of the 558-defect, since, due to the inverted spin-momentum locking between the Dirac bands on the two sides of the defect, backscattering is possible by a process where the charge carriers are scattered to the other side of the defect and propagate backwards without flipping the spin. The possible formation of 2D Dirac modes on 2D boundaries (do-

main or grain boundaries) in 3D TIs has only been hinted at in Ref. 14, but we anticipate that the preservation of the handedness of the surface modes may prove true also in these cases. Hence, from our result for a 1D boundary in a 2D TI, we expect inversion of the spin texture and the possibility of backscattering between Dirac modes on the two sides of 2D boundaries in 3D TIs.

$L$ (Å)	gap (eV)
12.5	0.452
20.0	0.237
27.6	0.129
35.1	0.071
50.7	0.026
58.2	0.011
99.45	0.001
57.4 (BiBL+558)	0.022
77.4 (BiBL+558)	0.005

TABLE I: Energy gap (in eV) for 2D Bi ribbons (ZBiNR) as a function of the ribbon width ( $L$  in Å). Last two entries show gap for Bi layers with extended 1D defect (BiBL+558) for two values of the distance between the 1D defect and its periodic images.

Below, we address numerically the interaction between the two sets of Dirac modes on each side of the 558-defect, and come to the conclusion that the line of dimers at the core of the defect strongly screens the interaction. We interpret this result as follows: the dimers introduce a potential barrier that leads to a much faster exponential decay of the Dirac mode from one side of the defect onto the other side. It is thus conceivable that backscattering between the two sides of the defect, as in the above picture, may be inhibited by the same mechanism.

We propose the following interpretation for the appearance of the Dirac cones in the BiBL+558 system: the region occupied by the 558-defect behaves topologically as a trivial insulating material, akin to the vacuum surrounding the edges of a bismuth ribbon. Furthermore, it has been determined by Wang et al. [23] that by saturating the edges of a ZBiNR with H atoms, the Dirac cones of topological edge states move from the K point in the case of unsaturated edges to the  $\Gamma$  point in the H-saturated-edge case. We observe the same behavior in the metallic states along the core of the 558-defect in a BiBL: the Dirac point for the pair of degenerate Dirac branches occurs at the  $\Gamma$  point. Hence, the line of Bi dimers in the core of the defect plays a role of saturation likewise that of hydrogens in a ZBiNR.

We will expand on the above interpretation in the following, but let us first analyze the nature of the interaction between the two pairs of Dirac modes on the core of the 558-defect.

We start from the behavior of the gap of the Dirac edge modes of a ZBiNR, due to the quantum tunneling

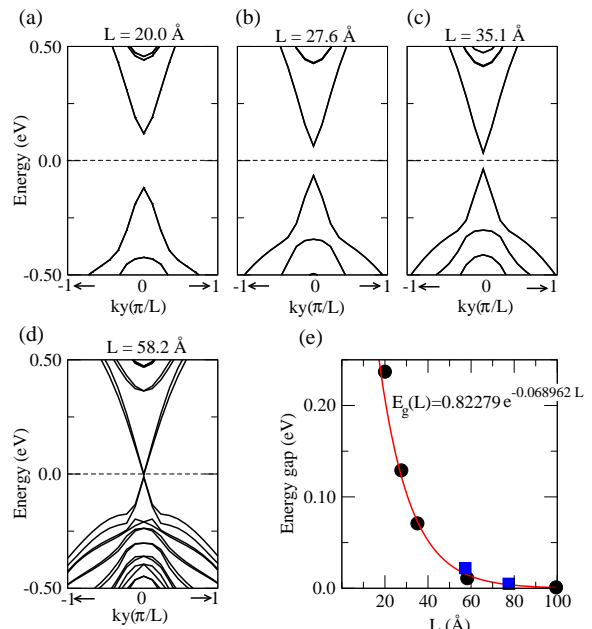


FIG. 2: (a)-(d) Electronic band structures of zigzag-edged Bi ribbons (ZBiNR), with widths ( $L$ ) ranging from 20 to 58 Å; (e) the band gap evolution of ZBiNRs as a function of  $L$ . Exponential fitting for  $\text{gap} \times L$  is shown. Blue squares show gap values for Bi layers with embedded 1D extended defect for two values of the distance between the 1D defect in the cell and its periodic images.

between the topological states with the same spin alignment in the two edges of the ribbon. The gap in the Dirac-fermion dispersion at the edges of the ZBiNR reflects the fact that the edge states penetrate into the bulk, with an exponential decay, and the interaction leads to the opening of a bonding-antibonding gap. As shown in Fig. 2 and Table I, as we increase the width of the ribbon the gap decreases, as expected. Figure 2(e), shows an exponential fitting of the ribbon gap as a function of the ribbon width ( $L$ ). For a  $\sim 58$  Å-wide ribbon the gap is 11 meV.

For the BiBL+558 system, due to the periodic boundary conditions of the supercell, a similar interaction due to the quantum tunneling is expected between the Dirac modes of the defect in the supercell and their neighboring periodic images. In the case of the ribbons, each edge interacts only with the other edge, while in the BiBL+558 the Dirac modes along the 558-defect core interact primarily with their two nearest periodic images, one to the right and the other to the left of the defect in the cell. The last two entries in Table I show the gap of the edge modes for the BiBL+558, for two different widths of the pristine region of the supercell. The gap for the supercell with a  $\sim 57$  Å-wide pristine region is 22 meV, twice the value for a ribbon this wide as included in Table I, which indicates that the interactions with the two periodic images add up.

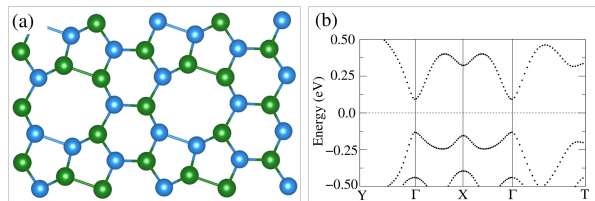


FIG. 3: (a) and (b) show a top of view and the band structure of a penta-hexa-octo form of a 2D Bi layer, respectively.

The above result is also suggestive of a very weak interaction between the two sets of Dirac modes in the core of the 558-defect, mediated by the line of dimers in the center of the core. In the BiBL+558, the distance between the edges on each side of the dimers is 5.35 Å. In order to investigate the nature of this interaction, we have also computed the gap in the Dirac modes for two H-saturated ribbons interacting through the vacuum in the same geometric configuration as in the BiBL+558 system, i.e., we removed the line of Bi dimers and kept the distance between the edges of the ribbons unchanged (at 5.35 Å). In this case, the gap increased by an order of magnitude to 134 meV. This result indicates that in the BiBL+558 the line of dimers strongly screens the interaction between the Dirac edge states. This is further confirmed by a calculation of the gap for a  $\sim 77$  Å-wide BiBL+558 system that yields a gap that falls on top of the exponential fitting for an isolated H-saturated ribbon, as shown by the red square in Fig. 2.

Let us go back now to our interpretation for the emergence of topological edge states along the core of the 558-defect. It rests on the assumption that the defect region acts as a portion of a trivial insulator. In order to confirm this picture, we compute the  $Z_2$  topological invariant for a pristine BiBL and for two “defective” Bi 2D layers. For a pristine BiBL, the  $Z_2$  has been obtained by looking at the parity of the occupied bands at the time-reversal-invariant momenta (TRIMs). We obtain  $Z_2 = -1$ , confirming its non-trivial topological character, with a band inversion at the M point. For a 2D bulk composed by a sequence of 558-defects connected by a stripe of single hexagons, as shown in Fig. 3(a), from the parity of the bands at the TRIMs we obtain  $Z_2 = 1$ , showing that, indeed, this stripe of a hypothetical penta-hexa-octo form of 2D Bi bilayers is a trivial insulator. The band structure for the penta-hexa-octo Bi bilayer is shown in Fig. 3(b).

A corollary of the above reasoning is that if we insert a stripe of a topological insulator as an extended 1D defect in a BiBL, we would see no Dirac cones of topologically-protected “edge” states along such a defect. In order to test this idea, we insert another extended defect, the quadruple pentagon-double octagon (Q5D8) defect, shown in Fig. 1(e), inside the BiBL. The Q5D8-defect is formed by two adjacent stripes of the 558-defect.

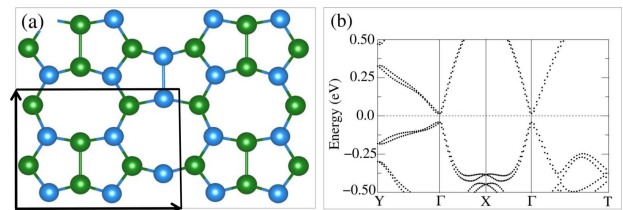


FIG. 4: (a) and (b) show a top of view and the band structure of a pentaoctite form of a 2D Bi layer, respectively.

As shown in Fig. 1(f), the Q5D8-defect does not introduce Dirac modes in the band gap of the BiBL, and a band gap is always present in the electronic structure of the BiBL+Q5D8 supercell. It follows that the Q5D8-defect can be seen as a finite portion of a Bi structure that belongs to the same non-trivial topological class as the pristine BiBL.

Although the 558-defect and the Q5D8 are both formed by pentagons and octagons, there is a crucial structural difference between the two defects. A pristine BiBL consists of two Bi triangular sublattices, labeled A and B, which are shifted by 1.74 Å in the perpendicular direction. In this geometry, each Bi atom in the “upper” (B) sublattice is bonded to three Bi atoms in the “lower” (A) sublattice, and vice-versa, as shown in Fig. 1(a). When we insert the Q5D8-defect in a pristine BiBL, all Bi-Bi bonds along the direction perpendicular to the defect are the same as in the pristine BiBL [a sequence of  $\text{Bi}_B\text{-Bi}_A$  bonds, see Fig. 1(e)], and this system belongs to the same topological class as the BiBL itself. On the other hand, the BiBL+558 system [see Fig. 1(c)] presents  $\text{Bi}_B\text{-Bi}_B$  and  $\text{Bi}_A\text{-Bi}_A$  bonds, which brake the A-B sublattice bonding pattern, and as a consequence it does not present a band inversion, and thus belongs to the class of trivial of insulators.

Our result for the electronic structure of the BiBL+Q5D8 system, suggests a striking conclusion, that an extended crystalline form of the Q5D8-defect should be a topological insulator. Based on that observation, we decided to investigate the topology of the electronic structure of a pentaoctite form of a BiBL, as shown in Fig. 4(a). In this geometry, the bilayer consists of buckled pentagons and octagons only. Figure 4(a) shows a  $2 \times 2$  cell of the pentaoctite BiBL. The rectangular box shows the 12-atom unit cell for this periodic structure. Indeed, this pentaoctite BiBL is an insulator, with a small gap of 0.035 eV, at the GGA level. From a calculation employing a hybrid functional we obtained a robust gap of 0.45 eV. For the calculation of the  $Z_2$  topological invariant of the Bi pentaoctite, we found it more expedient to employ the real-space methodology introduced by Soluyanov and Vanderbilt [24]. We obtain  $Z_2 = -1$ , confirming our expectation that the pentaoctite BiBL is a 2D topological insulator.

The fact that a hypothetical pentaoctite form of a Bi bi-

layer is a topological insulator naturally leads us to examine its possible experimental realization. In Table II, we show a comparison of the formation energy and atomic density of the bulk-derived hexagonal BiBL and of the pentaocite BiBL. The energy of the hexagonal layer is set to zero, for reference. The formation energy of the pentaocite BiBL is only 0.045 eV/atom above that of the hexagonal BiBL, i.e., the energy difference between the two phases is of the order of the thermal energy fluctuations per atom, at room temperature. Thus, from the energetics point of view the pentaocite BiBL is a viable crystalline phase. Table II also shows the atomic density of the two phases. The pentaocite BiBL is a less dense phase than the hexagonal layer, which indicates that a BiBL may undergo a phase transition to the pentaocite form under a tensile strain. The pathway for a hexagonal-BiBL  $\rightarrow$  pentaocite-BiBL transition will be the subject of a forthcoming publication.

structure	formation energy	atomic density
pristine	0.000	0.1231
pentaocite	0.045	0.1174

TABLE II: Formation energy (in eV/atom) and atomic density (in atom/Å<sup>2</sup>) of a bulk-derived hexagonal bismuth bilayer (BiBL) and of a pentaocite form of the BiBL. Formation energy of the hexagonal layer is set to zero.

In conclusion, *ab initio* DFT calculations indicate the formation of helical Dirac-fermion metallic states localized on the core of an extended 1D defect embedded in the bulk of a single (111)-oriented bismuth bilayer (BiBL). The formation of topologically-protected metallic states on the core of the 1D defect is related to the emergence of such metallic states along the edges of sufficiently large Bi ribbons. The core of the extended defect in our study is composed of two zigzag chains of Bi atoms connected by a roll of Bi dimers, forming the periodic unit of the defect, consisting of one octagonal and two pentagonal rings. The two zigzag lines of Bi atoms on the core of the 1D defects act as two zigzag edges, each edge hosting a pair of Dirac-fermion metallic modes, with linear dispersions.

Numerical DFT results show that the interaction between the Dirac modes on the two sides of the defect is strongly screened by the roll of Bi dimers at the geometric center of the 1D defect core. The handedness of the two zigzag “edges” meeting at the core of the 1D defect is preserved, which leads to an inversion of the spin-momentum locking between the two pair of Dirac modes localized on the 1D defect: spin ‘up’ (‘down’) modes propagate up (down) on one side of the defect and down (up) on the other side, which leads to the possibility of backscattering between the Dirac modes, induced by disorder in the region of the 1D extended-defect core.

Moreover, we also introduce an alternative crystalline

form of a Bi bilayer, consisting entirely of pentagonal and octagonal rings, which we refer to as the pentaocite form of a Bi bilayer. The formation energy of the pentaocite Bi bilayer is only 0.045 eV/atom larger than that of the bulk-derived hexagonal layer, and its density is slightly larger than that of the hexagonal layer, indicating a possible structural transition between the two 2D crystalline phases at moderate imposed tensile biaxial strains. Computation of the  $Z_2$  topological invariant shows that the pentaocite BiBL is a 2D topological insulator.

---

\* Current address: Departamento de Matemática, ICEN, Universidade Federal de Mato Grosso, Rodovia Rondonópolis-Guiringa, KM 06 (MT-270), Sagrada Família, 78735-910, Rondonópolis, MT, Brazil; Electronic address: erikanascimento@ufmg.br

† Electronic address: rwnunes@fisica.ufmg.br

- [1] C. L. Kane and E. J. Mele, Phys. Rev. Lett. **95**, 146802 (2005).
- [2] C. L. Kane and E. J. Mele, Phys. Rev. Lett. **95**, 226801 (2005).
- [3] M. Z. Hasan and C. L. Kane, Rev. Mod. Phys. **82**, 3045 (2010).
- [4] B. A. Bernevig, T. L. Hughes, and S.-C. Zhang, Science **314**, 1757 (2006).
- [5] M. König, S. Wiedmann, C. Brne, A. Roth, H. Buhmann, L. Molenkamp, X.-L. Qi, and S.-C. Zhang, Science **318**, 766 (2007).
- [6] D. Hsieh, D. Qian, L. Wray, Y. Xia, Y. S. Hor, R. J. Cava, and M. Z. Hasan, Nature **452**, 970 (2008).
- [7] I. Garate and M. Franz, Phys. Rev. Lett. **104**, 146802 (2010).
- [8] J. Chen, H. J. Qin, F. Yang, J. Liu, T. Guan, F. M. Qu, G. H. Zhang, J. R. Shi, X. C. Xie, C. L. Yang, et al., Phys. Rev. Lett. **105**, 176602 (2010).
- [9] J. G. Checkelsky, Y. S. Hor, R. J. Cava, and N. P. Ong, Phys. Rev. Lett. **106**, 196801 (2011).
- [10] J. Lahiri, Y. Lin, P. Bozkurt, I. I. Oleynik, and M. Batzill, Nature Nanotechnology **5**, 326 (2010).
- [11] J. H. Chen, G. Autès, N. Alem, F. Gargiulo, A. Gautam, M. Linck, C. Kisielowski, O. V. Yazyev, S. G. Louie, and A. Zettl, Physical Review B **89**, 121407 (2014).
- [12] S. S. Alexandre, A. D. Lúcio, A. H. Castro Neto, and R. W. Nunes, Nano Letters **12**, 5097 (2012), URL <http://pubs.acs.org/doi/abs/10.1021/nl3017434>.
- [13] L. C. Gomes, S. S. Alexandre, H. Chacham, and R. W. Nunes, J. Phys. Chem. C **117**, 11770 (2013), URL <http://pubs.acs.org/doi/abs/10.1021/jp400420m>.
- [14] Z. Y. A. Ran Y., Nat. Phys. **5**, 298303 (2009).
- [15] G. Kresse and J. Furthmüller, Phys. Rev. B **54**, 11169 (1996).
- [16] P. E. Blöchl, Phys. Rev. B **50**, 17953 (1994).
- [17] J. P. Perdew, K. Burke, and M. Ernzerhof, Phys. Rev. Lett. **77**, 3865 (1996).
- [18] S. Murakami, Phys. Rev. Lett. **97**, 236805 (2006).
- [19] M. Wada, S. Murakami, F. Freimuth, and G. Bihlmayer, Phys. Rev. B **83**, 121310 (2011).
- [20] Z. Liu, C.-X. Liu, Y.-S. Wu, W.-H. Duan, F. Liu, and J. Wu, Phys. Rev. Lett. **107**, 136805 (2011).

- [21] T. Hirahara, G. Bihlmayer, Y. Sakamoto, M. Yamada, H. Miyazaki, S.-i. Kimura, S. Blügel, and S. Hasegawa, *Phys. Rev. Lett.* **107**, 166801 (2011).
- [22] F. Yang, L. Miao, Z. F. Wang, M.-Y. Yao, F. Zhu, Y. R. Song, M. Wang, J.-P. Xu, A. V. Fedorov, Z. Sun, et al., *Phys. Rev. Lett.* **109**, 016801 (2012).
- [23] Z. F. Wang, L. Chen, and F. Liu, *Nano Letters* **14**, 2879 (2014).
- [24] A. A. Soluyanov and D. Vanderbilt, *Phys. Rev. B* **83**, 235401 (2011).